NASA TECHNICAL NOTE

NASA TN D-4118

NASA TN D-4118
c. 1

DEDUCTION OF REENTRY PLASMA PROPERTIES ABOUT MANNED ORBITAL SPACECRAFT FROM RADIO SIGNAL ATTENUATION DATA

by Paul W. Huber

Langley Research Center
Langley Station, Hampton, Va.

NATIONAL AERONAUTICS AND SPACE ADMINISTRATION • WASHINGTON, D. C. • AUGUST 1967

NASA TN D-4118

DEDUCTION OF REENTRY PLASMA PROPERTIES ABOUT MANNED ORBITAL SPACECRAFT FROM RADIO SIGNAL ATTENUATION DATA

By Paul W. Huber

Langley Research Center
Langley Station, Hampton, Va.

NATIONAL AERONAUTICS AND SPACE ADMINISTRATION

For sale by the Clearinghouse for Federal Scientific and Technical Information
Springfield, Virginia 22151 – CFSTI price $3.00

DEDUCTION OF REENTRY PLASMA PROPERTIES ABOUT MANNED ORBITAL SPACECRAFT FROM RADIO SIGNAL ATTENUATION DATA

By Paul W. Huber
Langley Research Center

SUMMARY

Comparisons of electron concentration deduced from flight reentry radio attenuation measurements from the Mercury and Gemini manned orbital reentries with those derived from theoretical models of reentry plasmas have been made. These comparisons indicate that the reentry signal loss profile typically associated with these spacecraft is attributable in large part to the effects of ablation impurities in the near-wake viscous flow regions.

The separated flow region generally exhibits the highest afterbody flow-field electron concentration as a result of two principal factors: (1) the finite-rate electron-ion recombination along afterbody inviscid flow streamlines is very effective in reduction of levels of electron concentration which are much above 10^{11} cm^{-3}; (2) the high static enthalpy and long flow dwell time associated with the separated flow region allow for large ionization of alkali ablation impurities introduced upstream in the heat-shield boundary layer.

The deduced ablation impurity levels in the near-wake viscous flow regions are much lower than those near the ablating heat-shield surface, apparently due to extensive afterbody mixing. Variation of a deduced mixing factor with Reynolds number based on body diameter indicates that shear-layer transition occurs at a Reynolds number of about 8×10^5 and that the afterbody flow is attached at Reynolds numbers less than about 2×10^4.

The introduction of small quantities of liquid spray into the separated flow can result in large decreases in the temperature and electron concentration of this region.

INTRODUCTION

It is a well-established fact that radio blackout of tracking and other communications occurs during atmospheric reentry from orbit of the large blunt-faced vehicles which typify manned spacecraft. It is also well understood that the source of this interference is the production of free electrons in the high-temperature ionized reentry

plasma about the spacecraft. (See ref. 1.) A number of empirical correlations have been made in the past which are reasonably successful in defining the regions, on a reentry map, where such blackout occurs. (See refs. 2 and 3.)

It has not yet been possible, however, to analytically describe the phenomena with regard to the fluid-mechanical and thermochemical nature of the plasma or the nature of electromagnetic propagation from the spacecraft antennas through the plasma. These shortcomings can be traced to two principal factors: (1) the geometric configuration of such a problem is in reality very much removed from those which are idealized and which are amenable to analytic fluid-mechanical or electromagnetic treatment and (2) the presence of ablation products from the heat shield involves a fluid-mechanics chemical-kinetics problem which is extremely complex and, at present, poorly understood. Studies in ground facilities are being made, but are limited to a few facets of the problem, or to greatly idealized conditions, because of the lack of ground simulation capability for the overall plasma electromagnetic wave propagation problem. (See ref. 4.) There has been, in recent years, a considerable amount of flight research aimed at an eventual understanding of the problem, but this has been confined, to date, to idealized configurations with nonablating surfaces. (See ref. 1.)

A considerable amount of received signal-strength data has been gathered from various ground-based tracking and communications stations in connection with the manned-spacecraft missions. These data, in some cases, can be sufficiently related to the spacecraft reentry flight parameters and orientations to provide the basis for an indirect diagnosis of the electromagnetic wave plasma interaction problem. For example, if the conditions were such that the wave propagation aspect of the problem could be represented by an idealized model, then the signal-strength data might be used to assess the plasma part of the problem or vice versa.

It is the purpose of this report to describe such a passive diagnosis of the plasma for Mercury and Gemini manned orbital reentry. Signal-strength data are used, along with data from ground facilities and theoretical models of the plasmas, to deduce the probable plasma properties and the types of flow-field plasma which contributed to the observed effects. It has been found possible to define clearly the roles played by ablation products and the near-wake flow regions in this phenomenon. Because the near-wake flow is the input to the far-wake problem, such knowledge might also prove useful for an improved understanding of the far-wake plasma properties of blunt ablating reentry vehicles. Furthermore, because of the similarity between blunt-body flow and flow over slender bodies at high angle of attack, this knowledge may also have application to lifting-body reentry plasma problems.

SYMBOLS

f	signal frequency, Hz
G	electronic degeneracy term (see eq. (8))
h	enthalpy
m	mass
M_∞	flight Mach number
M	molecular weight
N_e	electron concentration, cm^{-3}
N	part of Saha equation (see eq. (8))
p	pressure
Q	cross section for momentum exchange with electron, cm^2
$R_{\infty,D}$	Reynolds number based on maximum body diameter and free stream
S	distance along flow streamline (from shock, when no subscript)
T	temperature, ^oK
u	flow or vehicle velocity, ft/sec, km/sec
V	species ionization energy, eV
$\overline{V}$	effective ionization energy, eV
x	mole fraction
y	distance from surface along normal to flow
α_∞	angle between longitudinal body axis and flight path

α	fraction of ionizable species singly ionized
σ	apparent mixing factor (see eq. (11))
ν	electron collision frequency, sec^{-1}
ω	angular frequency, $2\pi f$, radians/sec

Subscripts:

a	air
abl	ablation material
c	positive ion
e	electron
i	ionizable material
mix	mixture of air and ablation material
n	neutral
R	denotes length for recombination (from shoulder to antenna)
s	stagnation
w	wall
o	standard laboratory conditions (p_o = 1 atm, T_o = 273.2° K)
p	plasma

DATA FROM REENTRY OBSERVATIONS

Signal Loss

The radio signal loss data obtained during reentry of the manned orbital missions, Mercury and Gemini, are quite similar for each of these classes of orbital missions.

Data obtained for the MA-6 and GT-3 spacecraft reentries are presented in table I and are typical of the respective missions. A sketch of the reentry plasma flow regions for the GT-3 spacecraft is shown in figure 1, and the reentry velocity-altitude profiles for both missions are shown in figure 2. The reentry plasma flow regions for the MA-6 spacecraft (not shown) are quite similar to those of the GT-3 spacecraft except that the longitudinal body axis is alined with the flight path $\alpha_\infty \approx 0$, and the VHF antenna (bicone antenna) is on the cylindrical afterbody. The maximum body diameter for the Mercury spacecraft is 6.2 feet (1.9 m) and that of the Gemini spacecraft is 7.4 feet (2.3 m). It should be noted that the exact identification of an attenuation condition, as listed in table I, is subject to a certain arbitrariness in the interpretation of signal-strength records because of antenna pattern uncertainty, noise level, etc.

Electron Concentration

With the signal loss data, it is possible to deduce a peak shock-layer value of plasma electron concentration for each point listed provided that the corresponding electron collision frequency is known, and that a model of the electromagnetic wave propagation can be employed which is amenable to analysis and is reasonably valid for the flight configuration. For these reentry conditions (i.e., low collision frequencies and thick plasmas) it will be shown that the computed electron concentration is, fortunately,

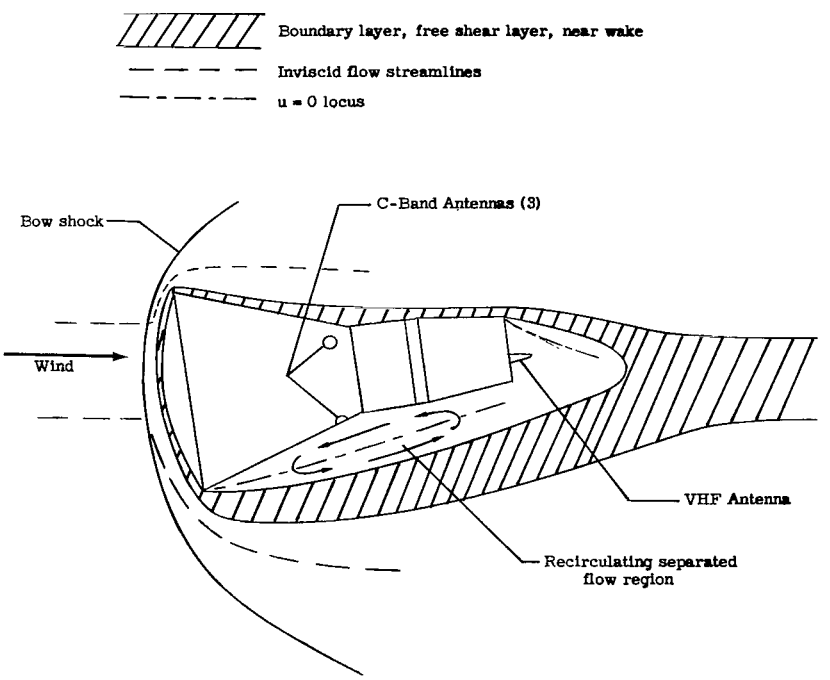

Figure 1.- Reentry plasma flow regions about the GT-3 spacecraft.

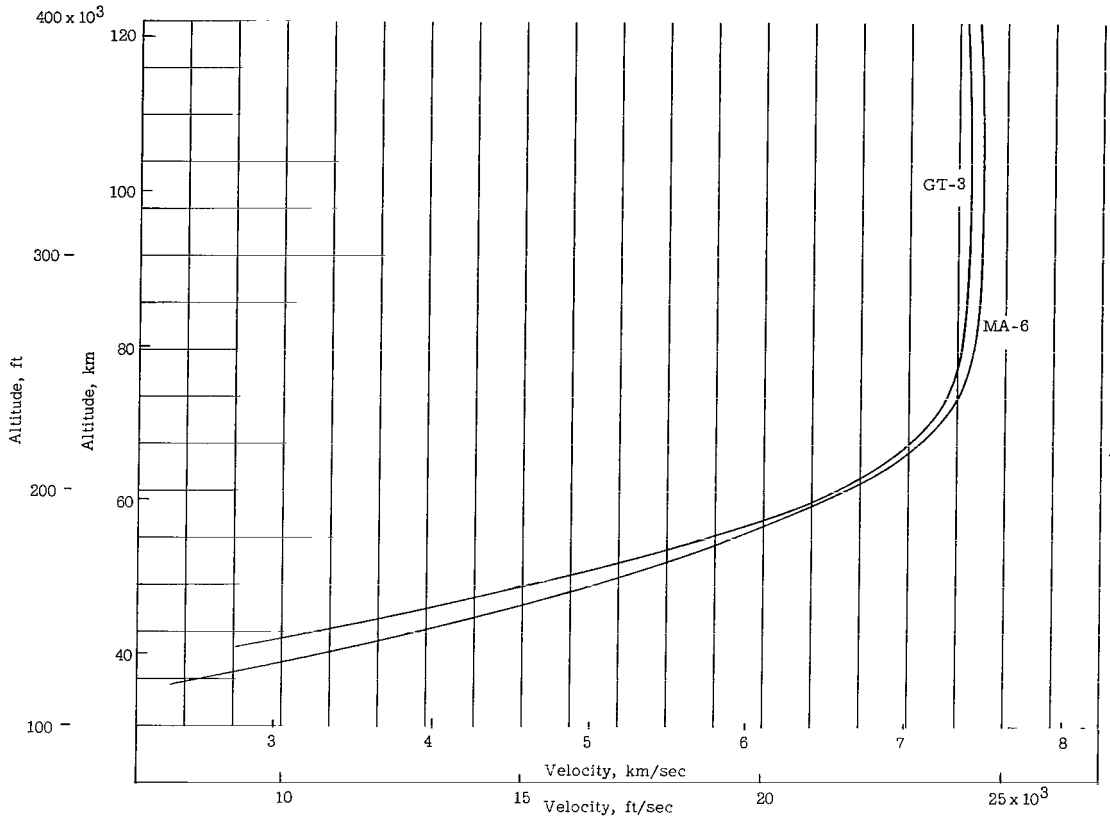

Figure 2.- Velocity-altitude reentry profiles for MA-6 and GT-3 spacecraft.

not very sensitive to collision frequency and plasma thickness. Approximate values are therefore used for a first guess, and if any significant sensitivity exists, an iteration based on the indicated plasma diagnosis (described in a later section) is employed. The collision frequency is first computed for an idealized air plasma by using the following approximate relation (ref. 5) for a two-species plasma (electron collisions with neutrals and positive ions):

$$\nu = 5 \times 10^{12} \frac{p/p_o}{T^{1/2}} \left(1 + x_e \frac{Q_c}{Q_n}\right) \tag{1}$$

where Q_n is herein assumed to be 1.1×10^{-15} cm^2, and Q_c is computed from the usual plasma physics relations for impact parameter and Debye shielding distance $\left(\frac{Q_c}{Q_n} \cong 10^3\right)$. The electron (or ion) mole fraction used in the long-range interaction correction term of equation (1) $x_e \frac{Q_c}{Q_n}$ is found from the following equation:

$$x_e = \frac{N_e T}{7.35 \times 10^{21} \frac{p}{p_o}} \tag{2}$$

where the constant in the denominator is the product of Loschmidt's number and T_0. The correction term in equation (1) is not very large for these cases and could be neglected without serious error. Also included, although not very important to the final iterated N_e, was a correction to the value of Q_n for indicated alkali impurities. The indicated impurity levels are discussed in a later section.

Knowledge of the flow-field temperature and pressure is required for evaluation of equation (1). Since the antennas for these spacecraft are located in the aft regions, the electromagnetic wave propagation path might be through the flow which is attached or separated – depending upon α_∞, $R_{\infty,D}$, and the roll orientation with respect to the receiving station. By considering the wind-tunnel and flight data for these configurations (refs. 6 and 7), a value of pressure coefficient of 0.015 of the stagnation pressure coefficient can be assumed as fairly representative of both the separated and attached aft inner flow for the purposes of these calculations. The aft flow temperatures were found for the separated and inviscid flows, respectively, from theoretical enthalpy estimates and finite-rate chemical-kinetics calculations, both to be described later.

A plane-wave slab model (see ref. 8, for example) was then used to relate the radio frequency attenuation change which occurs near the point where $\omega \approx \omega_p$ to a homogeneous value of N_e which would be representative of the highest values in the fairly broad profiles typical of these flow fields. This model should be reasonably valid near $\omega \approx \omega_p$ for thick plasmas and low collision frequencies, even when possible near-field antenna effects are considered. A thickness of 1 foot (30.5 cm) was assumed for the slab, since the flow-field calculations to be described later indicate thicknesses at least this large for the layers of high-entropy inviscid airflow as well as for separated flow regions. This assumption is not very critical since assumed thicknesses 50 percent larger or smaller resulted in a relatively small change in indicated N_e. Also, the assumption of one reflection or two reflections at the slab boundaries (one reflection, for the case of a very diffuse boundary on one side) made very little difference in N_e, except for the cases designated (b) in table I. In other words, even though several gross approximations are employed in the determination of N_e from the attenuation data, for most of the reentry range of collision and signal frequencies $\left(0.001 < \frac{\nu}{\omega} < 0.10\right)$ there is a rather sharp rise of attenuation near the point $\frac{\omega}{\omega_p} = 1.0$ (where most of the data points occur) for increasing ω_p; therefore, the deduced value of N_e is not greatly in doubt. The exceptions are the low-velocity VHF points $\left(\frac{\nu}{\omega} \rightarrow 0.50\right)$ where a more careful iteration is required.

The computed values of N_e are shown in table I for each attenuation condition. The uncertainties in the computation due to the various approximations which were made, as well as those involved in reading the records, are lumped into one factor which is also tabulated with N_e. The additional uncertainty due to antenna pattern was not

evaluated. It might be pointed out that the greatest single uncertainty is that due to lack of knowledge of temperature, since this property for inviscid flow differs greatly from that for viscous flow. Even so, this appears as $T^{-1/2}$ in equation (1), and for most cases the insensitivity to the collision frequency makes the uncertainty fairly small.

THEORETICAL ELECTRON CONCENTRATION FOR PURE AIR

As can be seen in figure 1, the value of N_e, which is deduced from the observations previously described, might be that existing in either of three aft flow regions – the inviscid flow, shear layer, or separated flow. It remains, therefore, to make such a determination by looking at some of the theoretical possibilities for each region.

Inviscid Plasma

The theoretical approach used for the inviscid flow plasma determination is one wherein chemical-kinetics is employed along flow streamlines, starting with the ambient air ahead of the vehicle bow shock and on through to the afterbody regions of the flow field. This program, along with results pertinent to the NASA Langley Research Center project RAM flight research vehicle, is described in reference 9, but for convenience some of the salient features will be mentioned. The matching parameter is pressure distribution along the streamline, and the other inputs are ambient velocity, pressure and temperature, and shock angle at the point of streamline entry. The flow field is constructed by computing several streamlines in the plane of symmetry for each flight condition, and then finding the profiles along normals to the shock layer flow. There is some uncertainty involved in specifying the exact location of streamlines in the afterbody region because of the separated flow and angle of attack. Fortunately, for these large blunt bodies, the plasma layers are thick and the profiles broad, so that the peak values of N_e are not seriously affected by the uncertainty in streamline location. The streamline pressure distributions and streamline locations used are based on consideration of surface pressure distributions, such as found in references 6 and 7, real-gas blunt-body solutions, such as references 10 and 11, and estimates of the separated flow detachment angles. The chemical-kinetics model used in the streamline program is one in which the shock compression is instantaneous and involves no chemical changes, but is otherwise in thermal equilibrium. This shock process is then followed by a chemical relaxation process of dissociation, ionization, charge transfer, and recombination which occurs through 36 finite-rate reaction paths involving 11 air species. Electron temperature is assumed to be that of the other gas species. At low densities (altitudes greater than about 250 000 feet (76.2 km) for Mercury and Gemini) the shock-layer electrons may not equilibrate with the sudden drop in flow temperature around the shoulder. The extra complexity of a two-temperature model can not be justified, however, since at high

altitude, large boundary-layer growth invalidates the use of an inviscid approach. In reference 9, essentially this same program was used to compute the inviscid flow about a blunted cone. Comparisons of calculated N_e were made with flight-measured values, and considerable confidence in the reaction rate knowledge was gained from the comparisons. The results of these calculations for the MA-6 and GT-3 reentry conditions are shown in figure 3, where the peak values of N_e for the flow field are plotted at two aft locations for the reentry: (1) the most forward antenna location ($S_R \approx 4$ ft (1.2 m) for

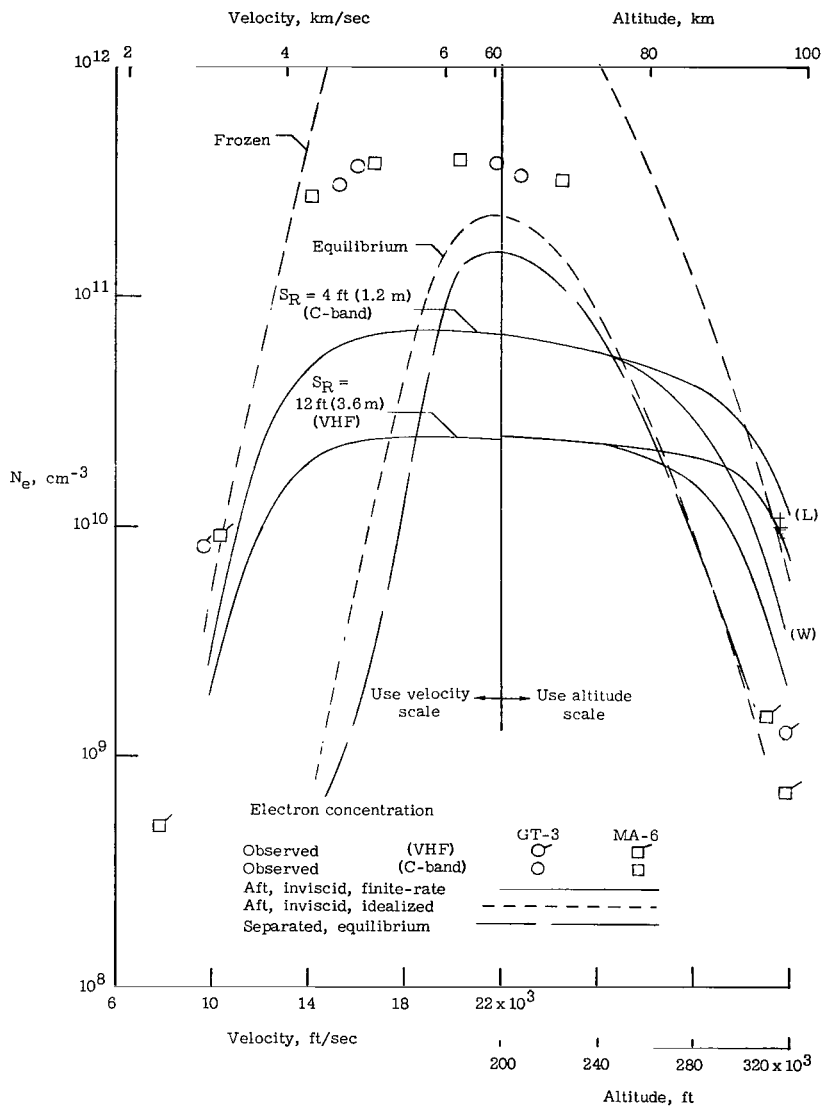

Figure 3.- Comparison of observed reentry electron concentrations with calculated values for a pure air plasma for MA-6 and GT-3 spacecraft. ((L), (W) denotes leeward, windward.)

Mercury C-band), and (2) the most aft antenna location ($S_R \approx 12$ ft (3.6 m) for Gemini VHF). For comparison purposes, the values of N_e for two idealized plasma models are also shown. These are for the maximum entropy inviscid streamline (along the body) for complete equilibrium (thermal and chemical), and for frozen flow (equilibrium stagnation point and frozen expansion). The flow-field pressure coefficient at both antenna locations is assumed to be 0.015 of the stagnation point value for all the curves plotted. The general influence of finite-rate chemistry on blunt-body reentry plasma properties is discussed in the appendix.

Note that the abscissa parameter in figure 3 is changed from altitude to velocity at the midpoint of the reentry. Even though this is somewhat unconventional, it is a very convenient means for representing the complete reentry on one plot and still maintaining the ability to visualize and compare differences in the ordinate values. Furthermore, the use of velocity in the latter part of reentry has been found to bring values of pure air N_e for the MA-6 and GT-3 spacecraft reentries much closer together than when plotted against altitude. Therefore, this method of presentation is also used in the subsequent plots of this report. When desired, figure 2, or table I, can be used to relate velocity to altitude at any point in the reentries.

Separated Flow Plasma

An approximate model for a separated flow plasma of pure air was also used and the results are shown in figure 3. In this model, the separated region is assumed to be in complete equilibrium and to have a uniform enthalpy, the value of which is prescribed by theoretical means and will be discussed later. Because of the long dwell time of this low-velocity recirculating flow, the equilibrium assumption is believed valid.

Shear-Layer Plasma

Theoretical calculations for the shear layers were not made because of the extreme complexity involved, but it seems physically reasonable that this plasma would not exhibit higher values of N_e than either the separated flow or the inviscid flow. This viewpoint is based on the premise that if additional ionization does occur in the shear layer (in addition to that in the inviscid flow) then the separated flow region should exhibit even more ionization since the temperatures are as high or higher, and the flow dwell time is much longer. This flow will be discussed in more detail later.

CORRELATION OF DATA WITH AIR PLASMA CALCULATIONS

Comparison of the observed values of N_e in figure 3 with the two more applicable models, finite-rate inviscid and equilibrium separated flow, shows that no real correlation

exists. The theoretical models are too low by at least a factor of 5 in the part of the reentry having high N_e as well as in the latter part of reentry. In the early high-altitude part where VHF attenuation begins, experimental values are close to the theoretical for the separated flow model and too low for good correlation with the finite-rate inviscid air model. Note that since the GT-3 spacecraft reentry is at angle of attack ($\alpha_\infty \approx 9^o$) both the leeward (L) and windward (W) flow results are shown. The bank angle (roll) at this time was such that the look angle to the north stations was mostly through leeward flow whereas that to the south stations was more through windward flow. For the MA-6 spacecraft, where $\alpha_\infty \approx 0$, the curves would lie between those shown. The effect of look angle will be discussed in more detail later.

Corrections to the inviscid finite-rate results for effects due to boundary layer, or shear layer, have not been made. Such corrections would apply at the very high altitudes (i.e., $>280 \times 10^3$ ft (85 km)) where the boundary-layer thickness at the nose is expected to be a large fraction of the total shock-layer thickness and hence have a significant effect on the complete flow field. At lower altitude, the boundary layer is thin relative to the shock layer, and such effects would not be significant for large blunt vehicles where the inviscid plasma layers with high N_e are thick. These boundary-layer corrections are extremely complex because of the finite-rate chemical reaction system required to account for nonequilibrium effects in the air which also contains large percentages of ablation impurities at the high altitudes where the corrections are important. It is conceivable, that if cold wall, pure air, boundary-layer corrections were made, the resulting matched inviscid, boundary-layer results might correlate with the observations of N_e at high altitude, since cold wall boundary layers in blunt-body flow fields usually lower the values of N_e (with respect to that of the inviscid case). (See ref. 9, for example.) It is more probable, however, that the correct model would include ablation products in the boundary layer.

EFFECTS OF ABLATION PRODUCTS

Because of the lack of correlation of observed values of N_e with the pure air plasma models, it seems to be a reasonable conclusion that pure air plasma is not responsible for the observed reentry signal attenuation throughout most of the reentry. The uncertainties in the observations (as discussed previously) and in the theoretical calculations (as demonstrated by the work of ref. 9) are much smaller than that required to account for the large difference seen in figure 3.

Since ablation of material from the heat shield does occur throughout the reentry period of interest, and since these materials are known to contain easily ionizable impurities it is necessary to consider the possible influence of such materials on the plasma properties. These theoretical considerations are limited to the separated flow plasma

only, since it is not expected that ablation materials would be found to a significant extent in the inviscid flow about the spacecraft, and since finite-rate chemical-kinetics computations of the shear-layer flow with impurities would be very complex and uncertain because of the lack of reaction and reaction-rate knowledge for such a mixture. On the other hand, the separated flow region is much more subject to analytical treatment of the ionization, if the assumption of equilibrium is valid and if the extent of ablation materials in this flow is known. Furthermore, it seems reasonable that the ionization is as great, or greater, in the separated flow than in the shear layer, since the temperatures (as will be shown) are as high, or higher, for the bulk of the reentry, the ablation content believed to be as high, and the flow dwell time definitely much greater. The latter factor is the justification for use of an equilibrium assumption.

Separated Flow Conditions

To compute the properties of the equilibrium separated flow plasma, it is necessary to know the pressure and temperature, as well as the composition in this region. From pressure measurements for blunt reentry bodies it has been found that the separated flow region is one of nearly constant pressure. A value of pressure coefficient of 0.015 of the stagnation pressure coefficient is a reasonable value (refs. 6 and 7) and was used for these computations. Temperatures appropriate to this region are estimated by using an enthalpy parameter and Reynolds number dependence as obtained from the theoretical analysis of reference 12 for the laminar rear stagnation-point enthalpy behind circular cylinders in hypersonic air. The resulting data, converted to a normalized enthalpy difference parameter $\frac{h - h_w}{h_s - h_w}$, is shown in figure 4 as a function of $R_{\infty,D}$. The dashed lines are arbitrary extrapolations of the reference 12 results made herein in order that the curve will apply to the complete range of GT-3 and MA-6 spacecraft reentry Reynolds numbers. Also shown are experimental data for blunted cones in air at $M_\infty = 12.8$ taken from reference 13 for two values of bluntness ratio (ratio of nose radius to body radius). It is seen that the enthalpy is sensitive to the bluntness ratio (for a cylinder, the ratio is 1.0) and that for very blunt shapes, such as the Gemini and Mercury spacecraft, the values might be even higher than for the cylinder. On the other hand, the bulk average value of enthalpy in the separated region will be lower than that of the rear stagnation point, since the enthalpy drops from the stagnation-point value to the wall value in surveys through this region toward the model base, according to references 12 and 13. Therefore, the cylinder data shown in figure 4 were used as a "best guess" in the separated flow calculations of the Gemini and Mercury models and is applied to both the base flow (VHF for Gemini) and body flow (C-band and VHF for Mercury) regions. Possible effects of corner radius on the separated flow enthalpy have been neglected. The enthalpy data and the pressure coefficient for the separated flow region are then used to readily compute the

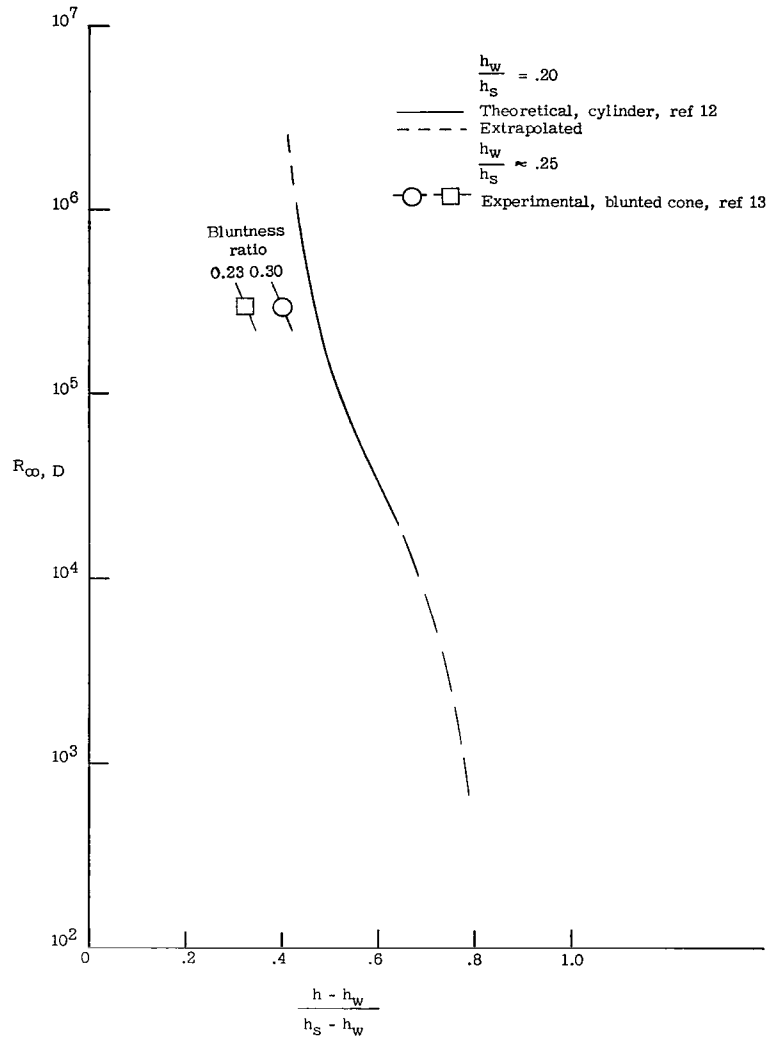

Figure 4.- Rear stagnation point enthalpy behind blunt bodies.

equilibrium pure air temperature for the reentries using real air thermodynamic charts such as reference 14. The resulting separated flow temperatures for air are plotted in figure 5 (curves labeled "pure air") and were used in estimating the separated flow curve for N_e previously given in figure 3.

Boundary-Layer Composition

The determination of the composition of the separated flow plasma with ablation is little more than a guess since there are no available mixing theories or experimental data which are quantitatively adequate for such a complex flow configuration. Some estimates are available, however, for the composition of the flow in the attached boundary

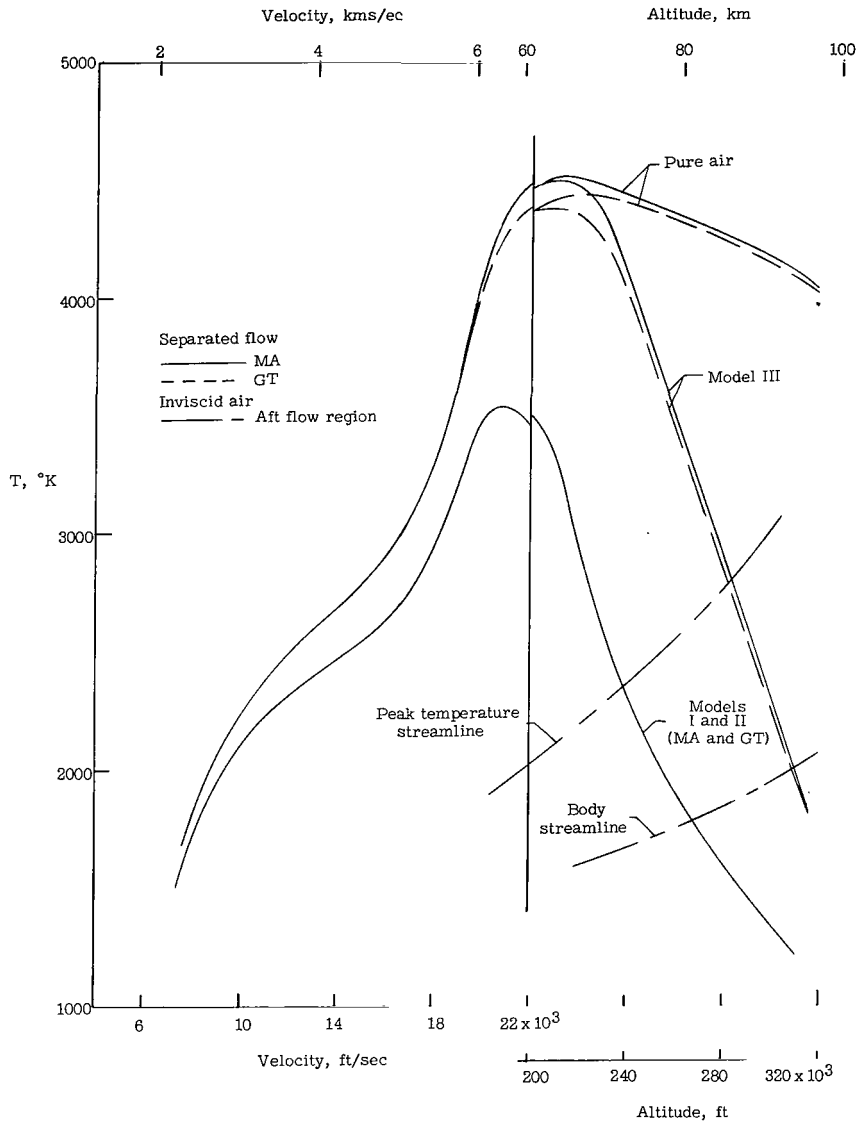

Figure 5.- Estimated equilibrium temperatures in Mercury and Gemini reentry separated flow regions for air-ablation mixtures.

layer on the heat shield. These estimates are based on ablation rates and boundary-layer mass flow rates and are used as a first guess for the separated flow composition. Three boundary-layer composition models are selected in order to better assess the significance of some of the assumptions and uncertainties involved. Two of these models (I and II) are for the estimated composition of the air-ablation mixture at the leeward heat-shield surface of the Gemini model before separation, and the other (III) represents an estimated composition obtained by assuming a uniform mixture of the leeward boundary-layer air and ablation material. These models are described in table II and figure 6. The

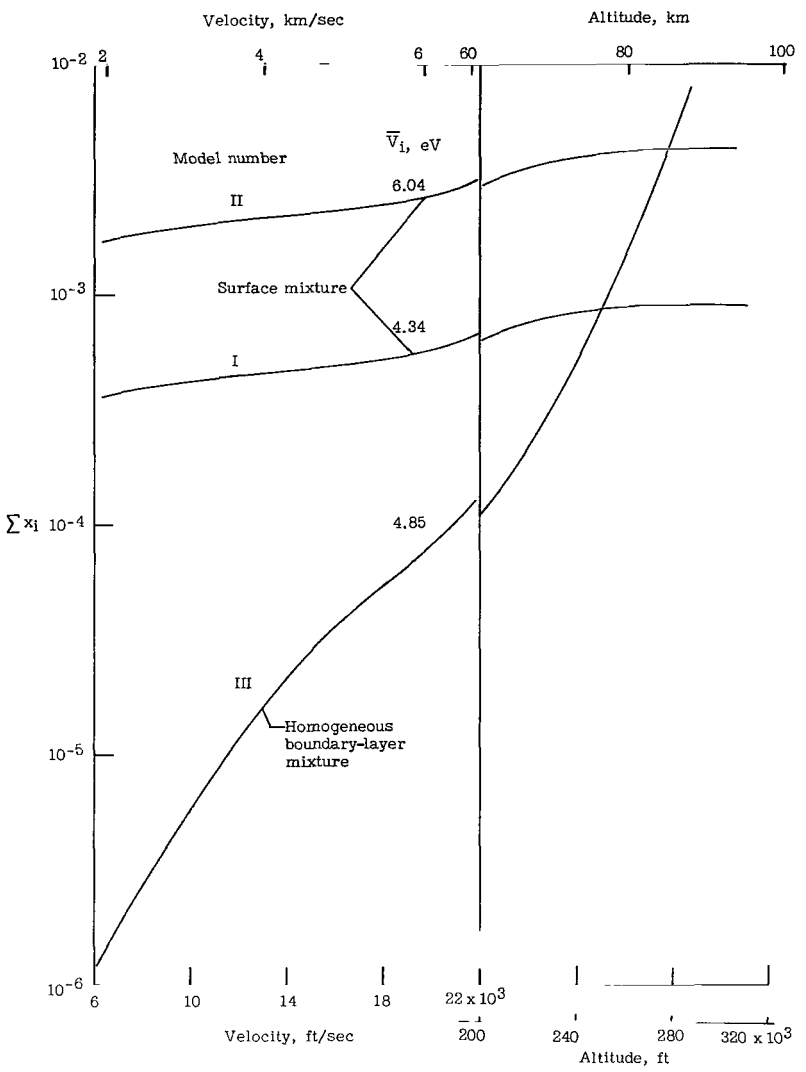

Figure 6.- Estimated alkali impurity in the heat shield boundary-layer air-ablation mixture for Gemini reentry.

ablation mass loss, alkali impurity, and boundary-layer air data from which models I and II were constructed were for a Gemini half-lift reentry trajectory which is quite similar to that of the GT-3 spacecraft. (Data obtained under Contract NASw-1209.)

Model III was constructed by using the ablation mass loss rate and impurity computed for the GT-3 spacecraft reentry along with the computed boundary-layer total air mass, in the same manner as was done in reference 15. Ablation estimates for the Mercury spacecraft were not available, but the differences to be expected due to trim angle and reentry trajectory were computed from blunt-face heating relations and the resulting values of $\sum x_i$ were found to be very close to those for Gemini when plotted as in figure 6. By using the parameters m_i/m_{abl} and m_{abl}/m_{mix} or m_{abl}/m_a as inputs, the values for $\sum x_i$ were computed herein from the following relations:

$$\sum x_i = x_{abl} \sum \left(\frac{m_i}{m_{abl}} \frac{M_{abl}}{M_i} \right) \tag{3}$$

$$x_{abl} = \frac{\frac{m_{abl}}{m_a} \frac{M_a}{M_{abl}}}{1 + \frac{m_{abl}}{m_a} \frac{M_a}{M_{abl}}} \tag{4}$$

$$\frac{m_{abl}}{m_a} = \frac{\dfrac{m_{abl}}{m_{mix}}}{1 - \dfrac{m_{abl}}{m_{mix}}} \tag{5}$$

$$\overline{V}_i = \frac{\sum(x_i V_i)}{\sum x_i} \tag{6}$$

where $M_{abl} = 4.5$, and the values for $\overline{V}_i$ were found from equation (6). The reason for the use of an effective ionization energy $\overline{V}_i$ for the ionizable species mixtures and of two different models from the same ablation-air data was purely for analytical expediency, since the Saha relation could be employed. When temperatures in the separated flow are less than about 3000° K, the alkali species such as potassium or sodium will contribute most of the electrons, and models I and III should be reasonable from this point of view. For temperatures greater than this, K and Na will be completely ionized and the other species will contribute additional electrons, so that model II will be more appropriate at these conditions.

Electron Concentration in Separated Flow With Boundary-Layer Composition

The electron concentration in the separated flow region is computed by using the composition (as a first guess) appropriate to the boundary layer on the heat shield before separation, described by the three models already discussed. The temperature of the separated flow air-ablation mixture is assumed, as a first guess, to be that given by the relation

$$T_{mix} = T_a - (T_a - T_w)\frac{m_{abl}}{m_{mix}} \tag{7}$$

which assumes that the specific heat of the ablation gases is equal to that of the air and that their temperature, before mixing, is T_w. The separated flow temperatures for the two reentries with ablation included are shown in figure 5, where models I and II are the same as far as m_{abl}/m_{mix} is concerned. Comparison of these temperatures with those for pure air shows only a small cooling effect for model III except at high altitude. A larger cooling effect is seen for models I and II in the high altitude part of the reentries, whereas the cooling effect decreases to a few hundred degrees in the later parts of reentry. It might be pointed out that recent data for separated flow afterbody heat transfer obtained at the NASA Ames Research Center (ref. 16) shows that afterbody heating decreases with increased forebody ablation rate. This decrease tends to support the concept of cooling due to ablation gases. Also shown in figure 5, for comparison, are the

aft finite-rate inviscid flow temperatures for the body streamline and for the peak flow field temperature streamline. Except for the high altitude part of reentry, it is seen that the separated flow temperatures are much higher than the inviscid. If a composition containing less ablation material than the boundary-layer mixture existed, then the separated flow temperatures would, of course, be even higher. The Saha relation for equilibrium single ionization of a single species ($\overline{V}_i$ herein) is then used to compute the ionization α of the effective ionizable species

$$\frac{\alpha^2}{1-\alpha} = \frac{\log^{-1}\left(2.5 \log T - 5040 \frac{\overline{V}_i}{T} - 6.49 + \log G\right)}{\sum x_i \frac{p}{p_o}} = \frac{N}{\sum x_i \frac{p}{p_o}} \tag{8}$$

where G is the electronic degeneracy term (see ref. 17). For the alkali species, $G = 1$; for Ca, $G = 4$; and for Al, $G \approx 1/3$ at these temperatures. The value was not found for Ti, but for simplicity the value of G in equation (8) was assumed to be unity for all three models. This assumption does not introduce any serious errors, since the resulting α would not be more than about 20 percent in error for the only model in question, model II. By next using the following relation

$$x_e = \alpha \sum x_i \tag{9}$$

along with equation (2), the electron concentration is readily determined. The results are shown in figure 7 for the Gemini and Mercury reentries using the temperature curves for each reentry as determined from figure 5. The observed values of N_e are shown for comparison. (See fig. 7(b).) The values of N_e for model III are not plotted for high altitude since this model is not valid when the boundary layer is very thick. For very thick boundary layers, the composition existing in the separated flow should approach that of the boundary-layer surface mixture; therefore, only models I and II are considered for high altitudes.

CORRELATION OF DATA WITH CALCULATIONS FOR AIR WITH ABLATION

Comparison of the values of N_e for model I with those of model II in figure 7(a) illustrates that for these temperatures (fig. 5) the species with the higher values of V_i are not important since N_e for model I is always as high, or higher. It was found that α computed for model II was always less than 0.25, whereas α for model I was near 1.0 in the region of high N_e. These results therefore suggest that model I is much more appropriate than model II for these reentries. For this reason only models I and III are plotted in figure 7(b) for comparison with the observed values. This comparison shows, first of all, that – whereas the pure air results in figure 3 were consistently lower than

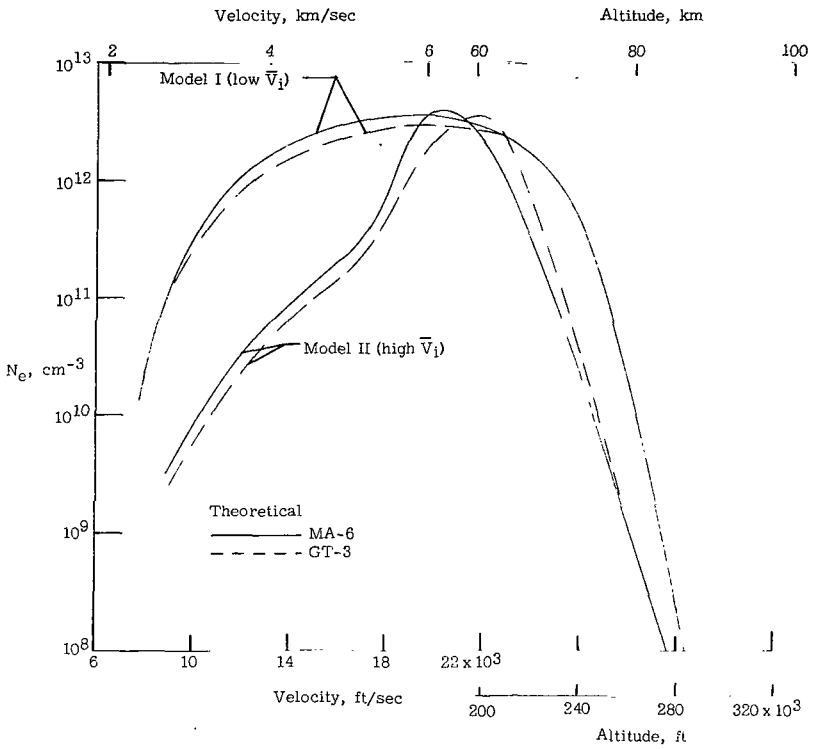

(a) Comparison of models I and II.

Figure 7.- Estimated electron concentration in the reentry separated flow region of Mercury and Gemini, assuming the composition is that of the heat-shield boundary layer.

observed – the ablation-air mixture yields values of N_e which are as high, or higher, than observed, except in the high-altitude region where the temperatures are greatly lowered because of ablation. Second, the comparison shows that N_e for the boundary-layer surface mixture is much too high for correlation in the C-band and low-velocity VHF regions, and that apparently a large reduction in the ablation mass fraction occurs in the mixing process in these regions. Large mixing is also suggested by the good correlation of the values of N_e for model III in these regions, and by the fact (see table II) that this model has a much lower boundary-layer ablation mass fraction.

It might be pointed out that in references 15 and 18, estimates were made of the Gemini reentry N_e for separated flow with ablation using values of V_i close to those of model III herein, arbitrary enthalpy assignments for the separated flow, and an assumed homogeneous heat-shield boundary-layer ablation-air composition. These estimates were made without consideration of the cooling effects of ablation on the mixture temperature. It is interesting, however, that the results are not significantly different from those computed herein for model III. This similarity suggests that for the

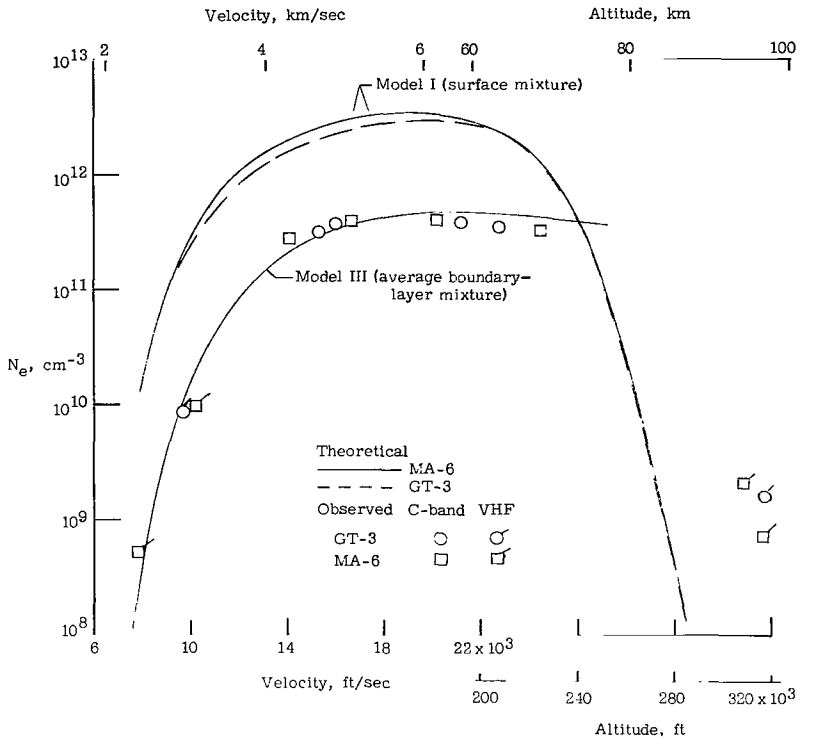

(b) Comparison of models I and III with observed values.

Figure 7.- Concluded.

easily ionizable species such as K and Na, which are in all cases near – or above – their ionization temperatures, the result is not critically dependent on the temperature value. For the species with higher values of V_i a greater temperature sensitivity exists, as seen from figure 7(a) for model II. The significant factor for these reentries therefore seems to be the alkali abundance $\sum x_i$.

EFFECTS OF VISCOUS MIXING IN AFTERBODY FLOW FIELD

The assumption of surface boundary-layer composition for the constituency of the separated flow (or for the inner shear layer, from which the separated region receives its fluid through diffusion and mixing) does not appear to be valid. For good correlation with the data, compositions much lower than those shown in figure 6 for model I are generally indicated.

Apparent Mixing

It is interesting to evaluate an apparent or observed value of $\sum x_i$ for the separated flow from the attenuation data for comparison with the values given in figure 6 for the ablation-air boundary-layer mixture. Such a comparison might give some indication of the magnitude of the mixing of gases in the shear layer along the dividing streamline and across the dividing streamline into the separated region. The process of mass entrainment into the shear layer and scavenging of mass from the separated flow region is, at best, very poorly understood for such an asymmetrical configuration and blunt shape as the Gemini spacecraft.

For this purpose, the observed value of N_e in table I is assumed to be representative of separated flow plasma, and the apparent x_e is then found from equation (2) by using the value of T_{mix} from equation (7) as a first guess for the temperature. With this temperature value and the value of $\overline{V}_i$ (appropriate to the composition model), the numerator of the right side of equation (8) is evaluated and denoted as N. Combining equations (8) and (9), and solving for $\sum x_i$ gives

$$\sum x_i = \frac{x_e^2}{N} \frac{p}{p_o} + x_e \tag{10}$$

for each attenuation point. For each of these trajectory points the ratio

$$\sigma = \frac{\left(\sum x_i\right)\text{boundary-layer composition}}{\left(\sum x_i\right)\text{apparent for separated flow}} \tag{11}$$

is then determined by using figure 6. The resulting ratios are plotted in figure 8 as a function of Reynolds number $R_{\infty,D}$ and represent the factors by which the boundary-layer alkali composition is apparently reduced by the mixing process before it is finally observed in the recirculating separated flow region. These are, of course, only very crude first estimates of the process because of the many assumptions and uncertainties involved.

Several deductions can be made immediately from the results of figure 8. First, a large mixing factor which increases with $R_{\infty,D}$ is indicated from the model I plots for the bulk of the reentry period. Second, there is a rather discontinuous change in slope of the mixing factor as a function of $R_{\infty,D}$ for both models at Reynolds numbers of approximately 8×10^5, indicating a greatly increased mixing at values higher than this. This discontinuity would appear to be a clear indication of transition from laminar to turbulent mixing at this point.

In addition to the indication of shear-layer transition by the sharp increase in mixing, the value of $R_{\infty,D}$ at which the mixing might be lowest, that is, where $\sigma \approx 1.0$, can be inferred very crudely. This value is obtained by extrapolating the data to low values of $R_{\infty,D}$, and it is found that the value of $R_{\infty,D}$ corresponding to $\sigma \approx 1$ is about 2×10^4. A straight line extrapolation is used for lack of valid low Reynolds number data. The VHF data would not be valid for this purpose since the VHF computed values of σ are much less than 1. Such a result merely means that the separated flow plasma could not have been responsible for the VHF data. It would seem to be indicated, therefore, that the flow might be attached on the afterbody surface at Reynolds numbers less than about 2×10^4 and would then, in fact, be the boundary-layer flow ($\sigma = 1$).

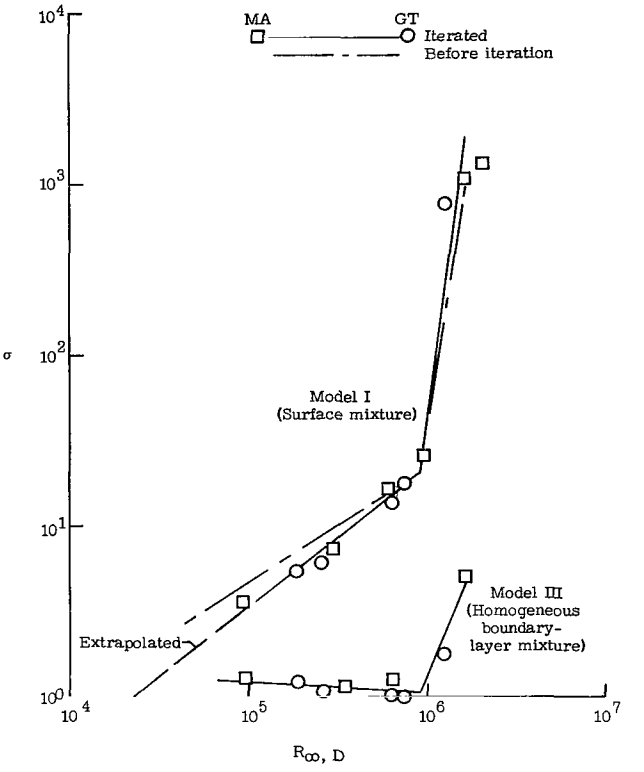

Figure 8.- Apparent ablation mixing and transition to turbulent flow in Mercury and Gemini shear layer and separated flow regions during reentry.

Viscous Flow Correlations

It is possible to support the previous implications about the nature of the afterbody viscous flow by comparison with measurements made in flight and in wind tunnels for these types of configurations. In reference 7, apparent transition on the MA-5 forward cone near the separation point was found to occur in flight at a value of about 8×10^5 for $R_{\infty,D}$. In reference 6, the injection of liquid spray into the windward inviscid flow field of a Gemini model at $M_\infty = 8$ was found to reduce the temperature in the separated base flow region. A significantly larger change in slope of separated flow enthalpy with injection rate occurred between $R_{\infty,D} = 6 \times 10^5$ and 1.1×10^6 than occurred between the other values of $R_{\infty,D}$, which might indicate that the mixing from the outer flow into the shear layer and separated flow increased more rapidly in that range. (However, other factors may be responsible.) Results of Gemini flight reentry transition measurements for the forward cone (ref. 19) indicate that $R_{\infty,D}$ is also about 8×10^5. Since the Gemini Spacecraft flight is at an angle of attack and the Mercury flight is not, the average

of the Gemini windward and leeward results is used for this comparison. The fluid existing in the separated flow is a result of mixing on all sides of this region.

Studies made at NASA Ames Research Center (ref. 20) with models of various shapes at hypersonic speeds showed that for models with body angles of 25° (roughly the angle for an average of the pertinent Mercury and Gemini flow angles) or higher, the attachment Reynolds numbers were about, or below, 3×10^4 for $R_{\infty,D}$. At $R_{\infty,D}$ much higher than this value the flow would probably be separated, and vice versa. Therefore, the implications from the attenuation data seem to be correct, even though the indications about the viscous flow advanced herein are not the result of measurements which are capable of directly indicating composition, transition, attachment.

It should be emphasized that the indications relative to near-wake viscous mixing and transition are not merely a consequence of – or even strongly dependent upon – the somewhat arbitrary enthalpy assignment which is necessary for the separated flow (fig. 4 and eq. (7)). This statement is based on the results of an independent calculation which was made for all parameters presented herein by using a completely different enthalpy assignment. This enthalpy had a Reynolds number dependency opposite that shown in figure 4, that is, higher enthalpy at high $R_{\infty,D}$ and much lower enthalpy at low $R_{\infty,D}$. The crossover point was at $R_{\infty,D} \approx 5 \times 10^5$. These results were essentially the same as those presented herein, even though the value of the air enthalpy parameter was much different at the high- and low-altitude VHF points. With respect to the C-band region, it has been pointed out previously that the alkali impurities K and Na are completely ionized, and changes in temperature produce only small changes in N_e. It seems to be shown rather clearly, therefore, that the entrainment, mixing, and scavenging which occur in the afterbody flow are significant factors in reducing those levels of alkali contamination appropriate to the heat-shield boundary layer to much lower values in the shear layer and separated flow regions. The reduction factors become large for laminar afterbody flow ($1 < \sigma < 15$) and very large for turbulent flow ($\sigma \gg 15$). It would furthermore appear from comparison of the data herein with reference 7 data for the trend of transition on the afterbody with $R_{\infty,D}$ (transition moving forward with increased $R_{\infty,D}$) that the transition which is significant to these attenuation results is that at about the most forward part of the shear layer (near the detachment point). It is interesting to note from the work of reference 21 that this type of transitional separated flow (transition occurring between the point of flow detachment and reattachment – if any) is both unsteady and markedly dependent on Reynolds number. These results seem to support the idea of greatly increased mixing with $R_{\infty,D}$ following transition.

It should be pointed out that because of the large mixing which is indicated from the results for model I in figure 8, it was necessary to make a second iteration of the temperature in equation (7), since the first guess was on the basis of the boundary-layer

composition. That is, since there is a much smaller fraction of low-enthalpy ablation gases in the separated flow mixture, the mixture temperature will be larger than that for the first guess (more like that of pure air as in fig. 5) for the C-band and low-velocity VHF regions. This iteration resulted in decreased values of σ as seen in figure 8. By using equations (3), (4), and (5), these indicated values are translated to those factors by which the ablation mass fraction is reduced by mixing, and the resulting values are from 1.0 to about 25 for laminar, and much greater values for the turbulent condition.

RELATIVE IMPORTANCE OF PLASMA MODELS UNDER DIFFERENT CONDITIONS

The data which have been presented give a strong indication that it is the separated flow (or possibly the inner shear layer) with ablation contamination and mixing which is responsible for the C-band attenuation and for the observed low-velocity VHF signal loss. (It is, of course, obvious that both the inviscid and separated flow plasmas have values of N_e high enough to cause VHF signal loss for a large part of these reentries. The question here is in regard to the plasma flow region pertinent to the observed signal loss and recovery data points.) As discussed earlier, the possible uncertainties involved in computation of the observed N_e from the signal loss data, or of the theoretical N_e in the inviscid flow chemical kinetics, are not large enough to account for the differences indicated in figure 3 (which stimulated this conclusion).

C-Band Region

Based on the knowledge gained herein, a tentative diagram of the leeward viscous flow plasmas is shown in figure 9 for the C-band part of the reentry. The properties at the boundary-layer edge in figures 9(a) and 9(b) are based on the finite-rate chemical-kinetics air results, and the properties in the separated region of figure 9(b) are based on the enthalpy and mixing models previously discussed. The balance of the properties and property profiles is only approximate and is, as stated, tentative. The important things to be noted here are that the highest values of T, N_e, and m_{abl}/m_{mix} are in, or near, the separated flow region. The temperatures in the inviscid afterbody flow are low because of the lack of neutral species recombination, and yet N_e is low because of very effective two-body electron-ion recombination along the streamline after the expansion at the shoulder (i.e., $S_R \cong 4$ ft (1.2 m)). A result such as this becomes evident only when the complete system of finite-rate processes are considered, since the frozen flow or equilibrium idealized models were shown to lead to serious numerical errors in the aft plasma properties (see fig. 3 and discussion in appendix). On the other hand, the enthalpy in the separated flow region is high, and this, coupled with the long flow dwell

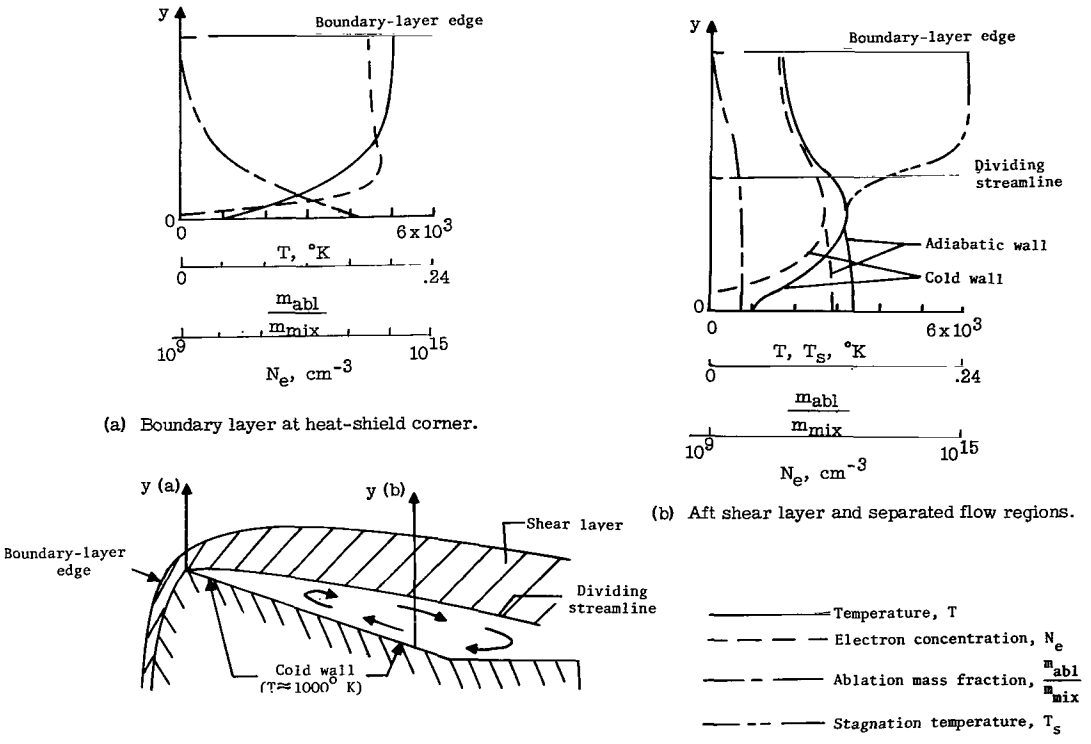

Figure 9.- Probable distributions of reentry plasma properties in leeward viscous flow regions at C-band attenuation.

time available, can lead to higher electron concentrations in this region when small amounts of ionizable impurities are present. As shown in figure 9(a), N_e in the inner part of the attached boundary layer is quite high (approximately 10^{14}) because of the large fraction of ablation material. When this flow expands in the afterbody shear layer, there is little likelihood of recombination of the alkali ions (three-body electron-ion recombination is required, but is very improbable at the densities of interest) so that, for the case of no mixing, N_e should be between 10^{12} and 10^{13}. However, values such as this would lead to an extended region of C-band blackout during reentry (which is contrary to the observations) and hence the concept of large mixing seems to be further substantiated on this basis. In other words, if the value of N_e corresponding to frozen alkali recombination is reduced by a factor of about 10 as a result of mixing, then N_e would be between 10^{11} and 10^{12} which would not be contrary to observation. The inner shear layer, therefore, cannot, on this basis, be ruled out as the plasma causing attenuation. Unfortunately, chemical-kinetic treatment of this region, along with viscous mixing, is too complex for presently developed theoretical analysis. In either event, it is interesting that the small amounts of alkali impurities in the afterbody flow are effective as tracers, or monitors, which enable an indirect diagnosis of the plasma to be made from the attenuation data.

It is also very interesting that the C-band frequency just happens to be ideally suited as a diagnostic tool for this range of N_e. If the electron concentrations were higher than 4×10^{11} cm^{-3}, complete blackout would have occurred, and if the levels of N_e were below about 1.5×10^{11} cm^{-3}, the attenuation would have been negligible. It was suggested (in results obtained under Contract NASw-1209) that the value of N_e may actually be higher than 4×10^{11} (in the shear layer) and that the C-band signals may find windows in the plasma at other locations via multiple-reflection paths. It is, however, difficult to specify what such paths might be to conform with the Mercury spacecraft observations, as well as with those of the GT-3 experiment described in the next section.

VHF Region

The indications relative to which plasma region is responsible for the high altitude VHF signal loss points are much less clear. As shown earlier, the inviscid pure-air plasma calculations yield values of N_e which are too high for correlation, but it is known that boundary-layer effects will be very large at these altitudes and render inviscid calculations very doubtful. Furthermore, with such thick boundary layers and ablation, pure-air approaches are not valid. On the other hand, it has been shown that, at these low Reynolds numbers, there probably will not be a separated flow region on the conical afterbody or cylinder. Even if there were a separated flow (i.e., as for the Gemini VHF antenna), the results presented herein considering ablation show that N_e would be too low because of the low temperatures. If this is the case, then the pertinent problem is that of a very thick contaminated afterbody boundary layer (or shear layer for Gemini VHF) which, again, is not presently amenable to good theoretical treatment because of the complex chemical kinetics and mixing phenomena. However, it is intuitively reasonable that the properties in such a plasma could produce the observed attenuations. Rough estimates of the properties are shown in the following sketch:

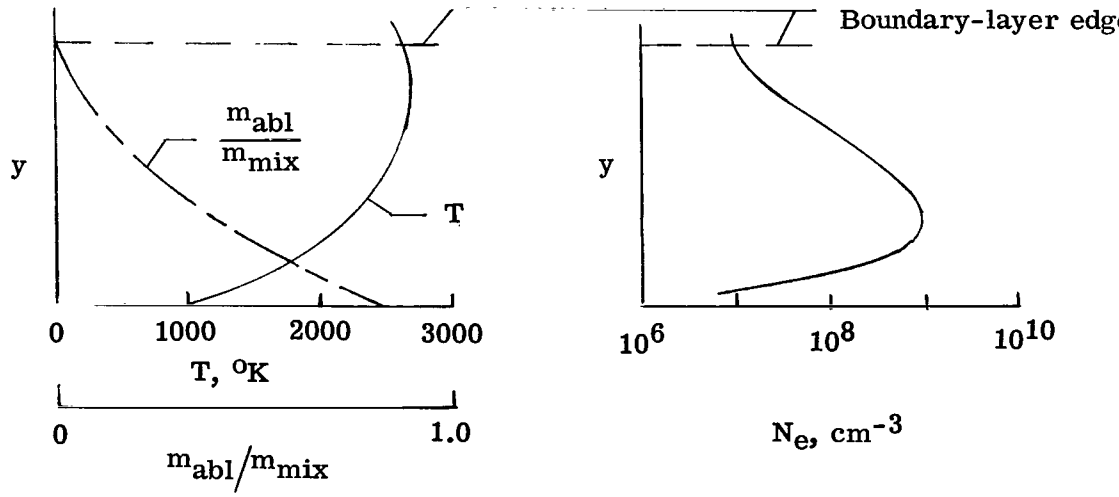

An electron concentration of the order of 10^9 cm^{-3} appears quite probable for such conditions when based on near equilibrium for the inner part of the boundary layer. Therefore, no positive conclusions can be made regarding the VHF blackout points at high altitude, except that it is a boundary-layer problem – either due to ablation contamination in the inner near-equilibrium portion of the boundary layer, or due to cooled pure air in the outer nonequilibrium boundary layer.

GT-3 Liquid Injection Experiment

It is possible to further strengthen the concepts relative to the role of afterbody mixing and separated flow plasmas in reentry radio interference by considering the results of a reentry communications experiment performed on the GT-3 mission. A complete description of this experiment is found in reference 22. In figure 10, a brief summary of the results pertinent to this discussion is presented along with a pictorial view of the reentry configuration. The view on the right is one which an observer would have from behind the reentering vehicle. To be noted are the locations of the three C-band antennas and the VHF stub antenna relative to ground receiving stations (arrows

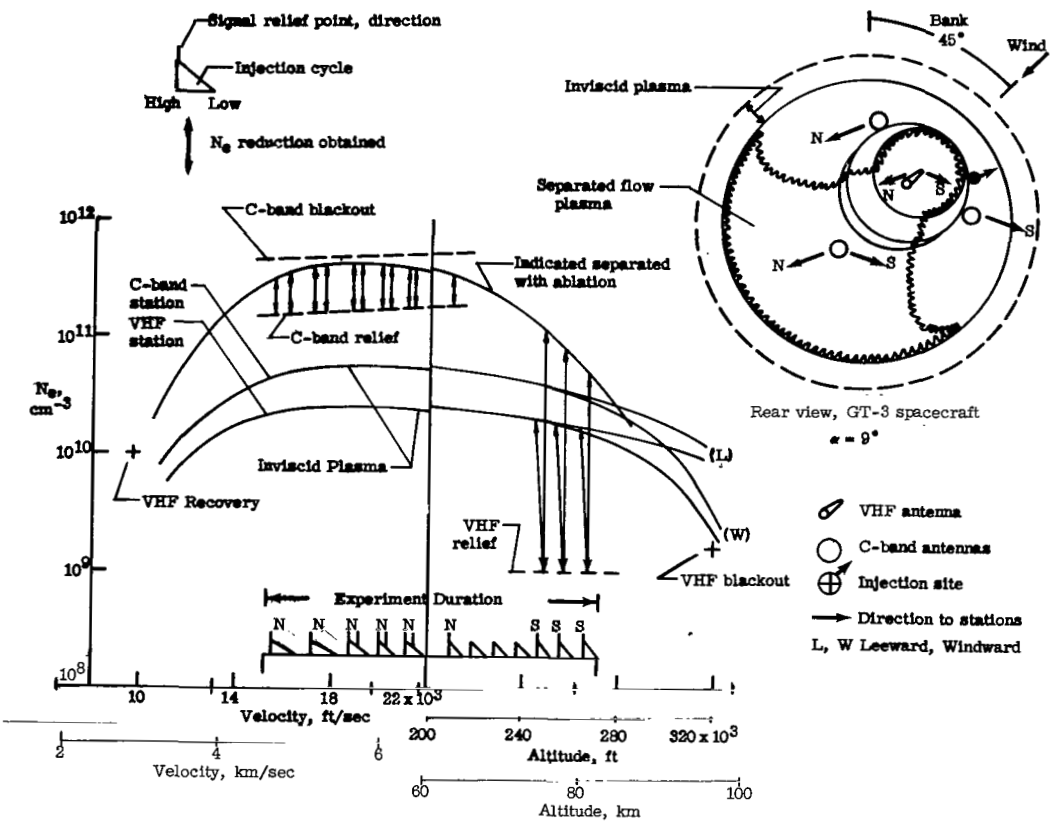

Figure 10.- Verification of separated flow plasma ionization from results of GT-3 injection experiment.

denote direction of south (S) and north (N) stations) and relative to the inviscid and separated flow plasmas. Inviscid plasma, of course, completely surrounds the vehicle, whereas the separated flow plasma is contained within the leeward afterbody flow region as approximately depicted by the wavy line. The injection site is on the windward side of the conical afterbody, a little aft of the midpoint of the conical section. The liquid spray nozzle was designed to inject forward into the inviscid air flow so that the droplets would be dispersed laterally upstream throughout the shock layer, but within a sector of the flow field on the windward side which would then act as a window (or slot in the plasma) for radio frequency transmission at the time of injection. Theoretical treatment of the probable mechanism of liquid-droplet-induced electron-ion recombination is found in reference 23, and a semi-empirical assessment of the mechanism, as derived from flight experiments, is given in reference 24. In the reentry plot of N_e in figure 10 are shown the theoretical inviscid flow, finite-rate calculations for the VHF and C-band antenna locations, as well as the results previously discussed herein for the probable values of N_e for the separated flow with ablation. At the bottom of the graph, the liquid injection pulses are shown at their corresponding reentry points as small right triangles. The triangles are merely idealizations of the actual cycles, each consisting of three discrete injections which were, chronologically, of low, medium, and high flow. (See ref. 22.) The left end of the triangle corresponds to the high flow-rate phase of the injection cycle. The flags on the triangles represent those injections which resulted in relief of signal attentuation, and the letters above the flags indicate the receiving station direction at which this relief was noted. The long vertical arrows on the graph represent the reductions of N_e in the plasmas which are required to produce the observed signal relief. For example, the first three high-flow injections resulted in VHF signal relief as seen from the stations to the south of the GT-3 reentry path. From consideration of the VHF stub antenna location and the values of N_e in the plasmas at this time, it becomes obvious that – irrespective of receiving station location – a large reduction of N_e in both plasmas is required, since propagation must be through both plasmas. The fluid injection, therefore, not only resulted in opening a window in the inviscid plasma on the windward (southerly) side of the vehicle, but furthermore, because of the mixing process, resulted in sufficient cooling of the separated flow region to lower the N_e to 10^9 cm^{-3} or less. The latter conclusion is not unreasonable in the light of the results of reference 6 which showed a large reduction of separated flow enthalpy with liquid injection into the inviscid flow, at injection rates much lower than these. It is furthermore not unreasonable in the light of the mixing results presented in figure 8, where the factor σ is indicated to be about 1.5 at this time in the reentry (at $R_{\infty,D}$ from 2.5×10^4 to 5×10^4 on the extrapolated line). No further relief of VHF was noted after this time, and this result is believed to be due to a lack of sufficient penetration of the liquid spray

through the inviscid shock layer at the higher reentry air densities (lower altitude). This conclusion is based on the post-flight analysis made in reference 6.

Later in the reentry, when N_e in the separated flow plasma with ablation becomes high enough to produce a significant C-band signal loss, there was observed to be a relief of attenuation corresponding to each high-flow and most of the medium-flow injections. This relief was observed at the north stations; there were no C-band receivers (active mode) in operation on the south side during reentry. If the location of the three C-band antennas on GT-3 spacecraft and of the separated flow region is now considered, it becomes obvious that the only antenna clearly engulfed in separated plasma is the one on the north side. The other two are shielded from the north stations by viscous plasma. Hence, it is quite likely that attenuation (and relief) would have been seen only from this direction, even if there had been C-band receivers to the south, since the south antenna is completely free of this plasma. (It is probable that if the vehicle had been rolling rapidly during the reentry, the received C-band signal attenuation would have been of a cyclic nature.)

This result of C-band relief of attenuation seems to clearly establish the role of separated flow plasma with its high values of N_e and of mixing of inviscid air into the shear layer and separated flow regions. In the first place, the attenuation cannot be due to inviscid plasma because the window is located to the south and relief would then only be seen to the south, even if the spray penetration were great enough at these altitudes (which it is not). Secondly, the liquid-laden inviscid air must enter the separated flow region and reduce N_e there, for relief to be seen from the north. If mixing were only into the shear layer, but not into the separated flow, then it would be difficult to explain the relief from the north, since the shear layer thus cooled is on the wrong side of the north C-band antenna, and all three antennas are still shielded by the uncooled shear layer to the north. On the other hand, if droplets can enter the separated region at any point, the recirculation process allows for distribution of the liquid within the region, as well as dwell times sufficient for droplet evaporation and cooling of the flow. Finally, the fact that the medium-flow injections gave C-band signal relief but not VHF relief is indicative of larger mixing factors at the higher Reynolds numbers corresponding to C-band. Consider that the absolute value of the reduction of N_e required for the observed relief of C-band is approximately 4×10^{11} cm^{-3} minus 1.5×10^{11} cm^{-3}, or a reduction of at least 2.5×10^{11} cm^{-3}, whereas that for VHF relief is no more than 1×10^{11} cm^{-3} minus 1×10^{9} cm^{-3}, or about 1×10^{11} cm^{-3} reduction. Therefore, the larger values of σ indicated in figure 8 for this range of $R_{\infty,D}$ ($5 < \sigma < 12$) seems confirmed by the larger reduction of N_e obtained with a smaller injection rate, when compared with the VHF case.

CONCLUSIONS

Correlations of electron concentration deduced from flight reentry attenuation measurements from the Mercury and Gemini manned orbital reentries with those derived from theoretical models of reentry plasmas have been made. Based on these correlations, several conclusions are reached with regard to the properties of the near-wake plasmas and their role in the reentry signal loss phenomenon.

1. The reentry signal loss profile typically associated with these spacecraft is attributable in large part to the effects of ablation impurities in the near-wake viscous flow regions. The possible exception is the high-altitude VHF attenuation which may be the result of finite-rate nonequilibrium pure air cooled by a thick boundary layer.

2. The separated flow region generally exhibits the highest afterbody flow-field electron concentration as a result of two principal factors: (1) the finite-rate electron-ion recombination along afterbody inviscid flow streamlines is very effective in reduction of levels of electron concentration which are much above 10^{11} cm^{-3}, and it is noted that the use of equilibrium or frozen flow assumptions in such a computation would not lead to this result; (2) the high enthalpy and long flow dwell time associated with the separated flow region allows for large ionization of alkali ablation impurities introduced upstream in the heat-shield boundary-layer flow at lower temperatures. The resulting electron concentration can be greater than 10^{11} cm^{-3}.

3. The levels of ablation impurities in the near-wake viscous flow regions are generally much lower than those levels near the ablating heat-shield surface with attached flow. This reduction can be by large factors and is believed to be due to mixing processes which occur in the shear layer and across the dividing streamline. The separated flow impurity level is much closer to that level computed by assuming the ablation averaged across the heat-shield boundary layer.

4. Variation of these apparent mixing factors with Reynolds number based on body diameter indicates that shear-layer transition occurs at a Reynolds number of about 8×10^5 and that the afterbody flow is attached at Reynolds numbers less than about 2×10^4.

5. The introduction of small quantities of liquid spray into the separated flow can result in large decreases in the temperature and electron concentration of this region.

Langley Research Center,
National Aeronautics and Space Administration,
Langley Station, Hampton, Va., March 6, 1967,
129-01-06-03-23.

APPENDIX

INFLUENCE OF FINITE-RATE CHEMISTRY

It is believed both interesting and important to discuss the general influence of finite-rate chemistry on the inviscid afterbody flow field properties of a blunt vehicle. As a result of a large number of computer studies involving several different body shapes with different reentry velocities over the complete reentry range (see also ref. 9), several conclusions of a general nature may be drawn. First, the idealized models of complete equilibrium or frozen flow seldom, if ever, describe the plasma correctly. Second, even though these models represent conceptual limits to the nonequilibrium problem (i.e., equilibrium implies infinitely fast reaction rates, whereas frozen flow implies zero rates) they do not provide numerical limits to the problem and hence will often not even bracket the correct values. Third, there does not appear to be any simple correlation factor by which the ideal models may be manipulated to approximate the more complex finite-rate results (for example, the ratio of equilibrium N_e at the nose to the finite-rate value at an aft station may vary by a factor of 30 over the Mercury and Gemini orbital reentries).

The reasons for these conclusions are discussed in simplified form as follows: chemical reactions generally proceed more rapidly at higher temperatures and densities. The approach to equilibrium is more likely, therefore, to occur at the nose of a vehicle than elsewhere, but even so, equilibrium does not occur in typical manned reentries except in the immediate vicinity of the stagnation point. The general lack of equilibrium conditions at the nose of a blunt reentry vehicle is due to low density levels in the early part of reentry and due to low temperature (low velocity) in the latter part. There is a nonequilibrium electron overshoot phenomenon (see ref. 25) which can occur in the velocity range between 15×10^3 and 30×10^3 ft/sec (4.6 and 9.2 km/sec) and can result in a value of N_e at the nose which is as much as three times above that of equilibrium. (The rest of the flow properties are far short of equilibrium, however; for example, the temperature is higher than equilibrium because of the lack of dissociation.)

When the nose plasma expands around the shoulder into the aft region, where temperature and density are much lower, there is almost no recombination of neutral atoms at manned reentry conditions so that the aft flow temperatures are much lower than would be found if recombination occurred. The ions and electrons, however, may or may not recombine depending upon the absolute value of N_e and on the recombination length S_R available. Such recombination can proceed effectively when $N_e \geqq 10^{12}$ cm^{-3}, such as in the first part of expansion (high N_e) or in the aft (long duration) flow. However, very little recombination takes place when $N_e \leqq 10^{11}$ as may sometimes be the case at the

end of the shoulder expansion process. This effect is referred to as N_e rate limiting and is seen in figure 3 as a flattened peak on the finite-rate reentry curves.

The overall reentry picture, therefore, is one in which values of N_e that are either higher or lower than equilibrium may be found in the aft flow; higher when the nose value is at or above the equilibrium value and expansion is rate limited, lower when the nose is far short of the equilibrium value (regardless of the type expansion) or when the nose value is near equilibrium and the rate limited N_e in the aft flow is less than the equilibrium value. Note, also, that there are some points in figure 3 where the finite-rate curves cross the equilibrium curve. Such points are, of course, fortuitous since the other flow properties (temperature, density, and composition) are far from equilibrium, and the danger for misinterpretation would be great if experimental N_e data were obtained only near such points.

The finite-rate N_e in the aft flow may also be higher or lower than the frozen flow values; higher when there is overshoot at the nose followed by an expansion in which there is N_e rate limiting or lower when the nose flow does not reach the equilibrium N_e or when there is a recombination of N_e in the expansion.

REFERENCES

1. Huber, Paul W.; and Sims, Theo E.: The Entry-Communications Problem. Astronaut. Aeron., vol. 2, no. 10, Oct. 1964, pp. 30-40.

2. Huber, Paul W.; and Evans, John S.: Prediction of Reentry Plasma-Sheath Properties. Proceedings of the NASA Conference on Communicating Through Plasmas of Atmospheric Entry and Rocket Exhaust, NASA SP-52, 1964, pp. 7-22.

3. Lehnert, Richard; and Rosenbaum, Bernard: Plasma Effects on Apollo Reentry Communication. Proceedings of the NASA Conference on Communicating Through Plasmas of Atmospheric Entry and Rocket Exhaust, NASA SP-52, 1964, pp. 51-68.

4. Huber, Paul W.; and Sims, Theo: Research Approaches to the Problem of Reentry Communications Blackout. NASA paper presented at Third Symposium on the Plasma Sheath (Boston, Mass.), Sept. 21-23, 1965.

5. Huber, Paul W.: Hypersonic Shock-Heated Flow Parameters for Velocities to 46,000 Feet Per Second and Altitudes to 323,000 Feet. NASA TR R-163, 1963.

6. Beckwith, Ivan E.; Bushnell, Dennis M.; and Huffman, Jarrett K.: Investigation of Water Injection on Models of Gemini Vehicle and Resulting Predictions for GT-3 Reentry Communications Experiment. NASA TM X-1200, 1966.

7. Weston, Kenneth C.; and Fitzkee, Archie L.: Afterbody Heat Transfer Measurements Obtained During Reentry of the Spacecraft of the Mercury-Atlas 5 Mission. NASA TM X-564, 1963.

8. Stratton, Julius Adams: Electromagnetic Theory. McGraw-Hill Book Co., Inc., 1941.

9. Evans, John S.; and Schexnayder, Charles J., Jr.: Analysis of Theoretical and Experimental Electron Concentrations for RAM B3 Flight. NASA TM X-1412, 1967.

10. Lomax, Harvard; and Inouye, Mamoru: Numerical Analysis of Flow Properties About Blunt Bodies Moving at Supersonic Speeds in an Equilibrium Gas. NASA TR R-204, 1964.

11. Katzen, Elliott D.; and Kaattari, George E.: Inviscid Hypersonic Flow Around Blunt Bodies. AIAA J., vol. 3, no. 7, July 1965, pp. 1230-1237.

12. Reeves, Barry L.; and Lees, Lester: Theory of Laminar Near Wake of Blunt Bodies in Hypersonic Flow. AIAA J., vol. 3, no. 11, Nov. 1965, pp. 2061-2074.

13. Muntz, E. P.; and Softley, E. J.: A Study of Laminar Near Wakes. AIAA J., vol. 4, no. 6, June 1966, pp. 961-968.

14. Moeckel, W. E.; and Weston, Kenneth C.: Composition and Thermodynamic Properties of Air in Chemical Equilibrium. NACA TN 4265, 1958.

15. Beckwith, Ivan E.; Bushnell, Dennis M.; and Huffman, Jarrett K.: Fluid Mechanics Aspects of the Gemini Reentry Communications Experiment. Conference on Langley Research Related to Apollo Mission, NASA SP-101, 1965, pp. 217-237.

16. Lee, George; and Sundell, Robert E.: Apollo Afterbody Heat Transfer and Pressure With and Without Ablation at M_∞ of 5.8 to 8.3. NASA TN D-3620, 1966.

17. Buchanan, Robert S.: Study of a Seeded Plasma. ARL 62-310, U.S. Air Force, Mar. 1962.

18. Huber, Paul W.: Research Approach to Reentry Communications Blackout. Conference on Langley Research Related to Apollo Mission, NASA SP-101, 1965, pp. 189-203.

19. Raper, Richard M.: Heat Transfer and Pressure Measurements Obtained During Launch and Reentry of the First Four Gemini-Titan Missions and Some Comparisons With Wind-Tunnel Data. NASA TM X-1407, 1967.

20. Kuehn, Donald M.; and Monson, Daryl J.: Attached and Separated Boundary Layers on Highly-Cooled, Ablating and Nonablating Models at M = 13.8. NASA TN D-4041, 1967.

21. Chapman, Dean R.; Kuehn, Donald M.; and Larson, Howard K.: Investigation of Separated Flows in Supersonic and Subsonic Streams With Emphasis on the Effect of Transition. NACA Rept. 1356, 1958. (Supersedes NACA TN 3869.)

22. Anon.: Manned Space Flight Experiments Symposium – Gemini Missions III and IV. 1965.

23. Evans, John S.: Charge Recombination on Water Droplets in a Plasma. NASA TM X-1186, 1965.

24. Beckwith, Ivan E.; and Bushnell, Dennis M.: Depletion of Free Electrons by Water Injection Into the Flow Fields of Hypersonic Vehicles. Third Symposium on the Plasma Sheath (Boston, Mass.), Sept. 21-23, 1965.

25. Lin, Shao-Chi; and Teare, J. Derek: Rate of Ionization Behind Shock Waves in Air. II. Theoretical Interpretations. Phys. Fluids, vol. 6, no. 3, Mar. 1963, pp. 355-375.

TABLE I.- MA-6 AND GT-3 OBSERVED REENTRY FLIGHT AND SIGNAL-ATTENUATION CONDITIONS

[$f \approx 2.6 \times 10^8$ Hz (VHF system); $f \approx 5.6 \times 10^9$ Hz (C-Band system)]

Geometric altitude		Relative velocity		Type signal attenuation	Deduced N_e, cm^{-3}	Reynolds number, $R_{\infty,D}$
ft	km	ft/sec	km/sec			
MA-6 conditions						
318 000	96.9	24 400	7.44	VHF (a)	$(7.0 \pm 2\ ) \times 10^8$	8.0×10^2
310 000	94.5	24 400	7.44	VHF (b)	$(1.5 \pm 0.4) \times 10^9$	1.38×10^3
225 000	68.6	23 400	7.14	C (a)	$(3.2 \pm 0.2) \times 10^{11}$	9.7×10^4
188 000	57.3	20 200	6.16	C (c)	$(3.9 \pm 0.1) \times 10^{11}$	3.0×10^5
162 000	49.4	16 700	5.09	C (c)	$(3.8 \pm 0.1) \times 10^{11}$	6.4×10^5
147 000	44.8	14 100	4.30	C (a)	$(2.8 \pm 0.4) \times 10^{11}$	9.6×10^5
128 000	39.0	10 200	3.11	VHF (b)	$(9.3 \pm 3\ ) \times 10^9$	1.66×10^6
118 000	36.0	7 800	2.38	VHF (a)	$(5.0 \pm 2\ ) \times 10^8$	2.1×10^6
GT-3 conditions						
318 000	96.9	24 150	7.36	VHF (b)	$(1.3 \pm 0.4) \times 10^9$	9.4×10^2
208 000	63.4	22 100	6.74	C (d)	$(3.4 \pm 0.2) \times 10^{11}$	1.9×10^5
198 000	60.4	21 200	6.46	C (e)	$(3.8 \pm 0.1) \times 10^{11}$	2.6×10^5
165 000	50.3	16 000	4.88	C (e)	$(3.7 \pm 0.1) \times 10^{11}$	6.4×10^5
161 000	49.1	15 300	4.66	C (d)	$(3.1 \pm 0.4) \times 10^{11}$	7.6×10^5
136 000	41.5	9 700	2.96	VHF (b)	$(8.2 \pm 3\ ) \times 10^9$	1.28×10^6

(a) Onset, or end (≈2 dB loss).

(b) Signal blackout, or recovery, point (≈50 dB loss).

(c) Onset, or end, of high signal loss (≈30 dB loss).

(d) Onset, or end (3 to 5 dB loss).

(e) Onset, or end, of moderate signal loss (≈20 dB loss).

TABLE II.- BOUNDARY-LAYER COMPOSITION FOR GEMINI MODELS

Model I (air-ablation mixture at heat-shield surface):	
$\frac{m_i}{m_{abl}}$ for ionizable impurity –	
K	0.008
$\overline{V}_i$, eV	4.34
$\frac{m_{abl}}{m_{mix}}$ for altitude of –	
300 000 ft (91.5 km)	0.92*
250 000 ft (76.2 km)	0.69
200 000 ft (61.0 km)	0.25
150 000 ft (45.7 km)	0.13
Model II (air-ablation mixture at heat-shield surface):	
$\frac{m_i}{m_{abl}}$ for ionizable impurity –	
K	0.008
Al	0.0072
Ca	0.0002
Ti	0.0226
$\overline{V}_i$, eV	6.04
$\frac{m_{abl}}{m_{mix}}$ for altitude of –	
300 000 ft (91.5 km)	0.92*
250 000 ft (76.2 km)	0.69
200 000 ft (61.0 km)	0.25
150 000 ft (45.7 km)	0.13
Model III (homogeneous boundary-layer air-ablation mixture):	
$\frac{m_i}{m_{abl}}$ for ionizable impurity –	
K	0.012
N_a	0.013
$\overline{V}_i$, eV	4.85
$\frac{m_{abl}}{m_{mix}}$ for altitude of –	
300 000 ft (91.5 km)	0.53
250 000 ft (76.2 km)	0.04
200 000 ft (61.0 km)	0.0055
150 000 ft (45.7 km)	0.00075

*Extrapolated.

"The aeronautical and space activities of the United States shall be conducted so as to contribute . . . to the expansion of human knowledge of phenomena in the atmosphere and space. The Administration shall provide for the widest practicable and appropriate dissemination of information concerning its activities and the results thereof."

—NATIONAL AERONAUTICS AND SPACE ACT OF 1958

NASA SCIENTIFIC AND TECHNICAL PUBLICATIONS

TECHNICAL REPORTS: Scientific and technical information considered important, complete, and a lasting contribution to existing knowledge.

TECHNICAL NOTES: Information less broad in scope but nevertheless of importance as a contribution to existing knowledge.

TECHNICAL MEMORANDUMS: Information receiving limited distribution because of preliminary data, security classification, or other reasons.

CONTRACTOR REPORTS: Scientific and technical information generated under a NASA contract or grant and considered an important contribution to existing knowledge.

TECHNICAL TRANSLATIONS: Information published in a foreign language considered to merit NASA distribution in English.

SPECIAL PUBLICATIONS: Information derived from or of value to NASA activities. Publications include conference proceedings, monographs, data compilations, handbooks, sourcebooks, and special bibliographies.

TECHNOLOGY UTILIZATION PUBLICATIONS: Information on technology used by NASA that may be of particular interest in commercial and other non-aerospace applications. Publications include Tech Briefs, Technology Utilization Reports and Notes, and Technology Surveys.

Details on the availability of these publications may be obtained from:

SCIENTIFIC AND TECHNICAL INFORMATION DIVISION

NATIONAL AERONAUTICS AND SPACE ADMINISTRATION

Washington, D.C. 20546